J. Condensed Matter Nucl. Sci. 8 (2012) 37–48

Research Article

Statistical Analysis of Unexpected Daily Variations in an Electrochemical Transmutation Experiment

Felix Scholkmann*

Biomedical Optics Research Laboratory, Division of Neonatology, University Hospital Zurich, 8091 Zurich, Switzerland

Tadahiko Mizuno

Hokkaido University, Center for Advanced of Energy Conversion Materials, Sapporo 060-0813, Japan

David J. Nagel

The George Washington University, Washington, DC 20052, USA

Abstract

In two electrochemical transmutation experiments, unexpected oscillations in the recorded signals with a daily period were observed for deuterium/palladium loading ratio (D/Pd), temperature (T) and pressure (P). The aim of the present study was to analyze the time courses of the signals of one of the experiments using an advanced signal-processing framework. The experiment was a high temperature (375 K), high pressure (750 kPa) and long-term (866 h $\approx$ 35 days) electrochemical transmutation exploration done in 2008. The analysis was performed by (i) selecting the intervals of the D/Pd, T and P signals where the daily oscillations occurred, (ii) filtering the signals to remove low-frequency noise, (iii) analyzing the waveforms of the daily oscillations, (iv) applying Ensemble Empirical Mode Decomposition (EEMD) to decompose the signals into Intrinsic Mode Functions (IMFs), (v) performing a statistical test on the obtained IMFs in order to identify the physically most meaningful oscillation mode, (vi) performing an power spectral analysis, (vii) calculating the correlations between the signals, and (viii) determining the time-dependent phase synchronization between the signals. We found that (i) in all three signals (D/Pd, T and P) a clear daily oscillation was present while the current density J did not show such an oscillation, (ii) the daily oscillation in T and P had similar waveforms and where anti-correlated to the oscillation in D/Pd, (iii) D/Pd and T had the highest correlation ($r = 0.7693$), (iv) all three signals exhibited phase synchronization over the whole signal length while the strongest phase synchronization took place between D/Pd and T. Possible origins of the daily oscillation were discussed and implications for further investigations and experiments were outlined.

Keywords: Daily oscillations, Diurnal oscillations, Electrochemical transmutation, Ensemble empirical mode decomposition, Intrinsic mode functions, Low-energy nuclear reactions, Phase synchronization, Signal correlating

*E-mail: Felix.Scholkmann@usz.ch; Tel.: +41-44-2559792; Fax.: +41-44-2554442

© 2012 ISCMNS. All rights reserved. ISSN 2227-3123

1. Introduction

Changes in the distribution of chemical elements and in their isotopic abundances where surprisingly reported to happen during electrolysis experiment using both heavy and light water [1–26]. The physical mechanisms of these low-energy transmutations processes are not yet understood. There are many indications that they are not based on conventional nuclear reaction mechanisms, especially since they took place at low energies. Therefore, the term “low-energy nuclear reactions” (LENR) was defined to refer to such kinds of nuclear reactions.

In two electrolysis experiments, besides the transmutations observed, an unexplained oscillation in the recorded signals (loading of deuterium (D) in a Pd lattice expressed as the D/Pd loading ratio, temperature and pressure) with a daily period (i.e. with a period of approx. 24 h) was observed [27]. This is surprising since it has been assumed that LENR were independent of the time of day.

To gain further insight into the daily oscillation, the aim of the present study was (i) to extend and refine the data analysis using the dataset with the best record of daily oscillations (the data set from the experiment conducted by Mizuno et al. [15] available, (ii) to discuss possible causes for the daily oscillations, and (iii) to outline the implications for further investigations and experiments.

2. Materials and Methods

2.1. Data

For the current analysis, we used the recorded data obtained by a high temperature (375 K), high pressure (750 kPa $\approx$ 7.4 times of the mean atmospheric pressure at mean sea level) and long-term (866 h $\approx$ 35 days) electrochemical transmutation experiment done in 2008 [5]. During the D/Pd loading, the following signals where recorded simultaneously: D/Pd loading ratio (D/Pd [%]), temperature (T [K]), pressure (P [atm]) and current density (J [A/cm^2]). All of these four signals where recorded inside the experimental flask. The sampling frequency of the signals was 0.25/h, i.e., every 4 h a measurement was done. The D/Pd loading ratio was determined by continuously measuring the pressure of the oxygen gas inside the electrolysis cell and relating this to the amount of deuterium incorporated into the Pd sample.

2.2. Data pre-processing

Visual inspection of the four signals revealed a daily oscillation in the D/Pd, T and P signals when the D/Pd loading was above approximately 90%. This period started after approximately 320 h and ended after approximately 760 h, spanning a time of 440 h. According to this observation, for the next steps of the analysis only the data in this interval where used. The current density J showed no oscillations; it had a constant value (J = 0.2 A/cm^2) over the whole time span.

In order to get rid of the low-frequency noise in the recorded signals, a finite impulse response (FIR) high-pass filer of order 20 and with a cut-off period of 57 h was applied to the signals. To avoid distortion of the phase of the signals due to the filtering, a zero-phase FIR filtering was realized by processing the input data in both the forward and reverse direction.

2.3. Waveform analysis

To analyze the waveforms of the daily oscillation, a block average was computed for all three signals by using the FIR-filtered version of the signals. The block average was calculated by segmenting the signals to intervals with duration of 24 h each, and calculating the mean and standard deviation of the block averaged signals for these intervals.

2.4. Ensemble Empirical Mode Decomposition and selection of intrinsic mode functions

In order to extract the daily oscillation from the signals optimally, an advance signal processing technique (Ensemble Empirical Mode Decomposition, EEMD) was used. It allows decomposing of the signals into characteristic oscillations modes (called Intrinsic Mode Functions, IMFs). EEMD is a further development of Empirical Mode Decomposition (EMD), first introduced 1998 by Huang et al. [28]. EMD can be regarded as a type of adaptive wavelet decomposition [29] or a time-varying filter bank consisting of band limited filters with band widths that vary in time [30,31]. EEMD is a truly noise-assisted data analysis (NADA) method [32].

The IMFs are calculated from the signals such way that they fulfil two conditions: (i) every IMF has the same number of extrema and zero crossings and (ii) each IMF is symmetric with respect to the local mean. The EMD calculation process (called the 'sifting process') is the following [28, 33–35]: (1) All local minima and maxima of the given signal $x(t) = \{x(t_i)|i = 1, 2, \ldots, N\}$ are identified, (2) the upper $e_u(t)$ and lower $e_l(t)$ envelopes of the signal are calculated by interpolating the local minima and maxima by a cubic spline function, (3) the mean of the two envelopes $m_i(t) = [e_l(t) + e_u(t)]/2$ is then subtracted from $x(t)$ which gives the first component: $h_i(t) = x(t) - m_i(t)$. The steps (1)–(3) are performed again on $h_i(t)$ until $h_i(t)$ is a function that fulfils the two described conditions defining an IMF.

If $h_i(t)$ fulfils the conditions, $h_i(t)$ is an IMF denoted as $c_i(t)$. The residual $r_i(t) = x(t)–c_i(t)$ is then treated as a new signal and the sifting process is applied on it.

Finally, the original signal $x(t)$ is given as a sum of the IMFs and the residual:

$$x(t) = \sum_{i=1}^{M} c_i(t) + r_N(t),$$

where $c_i(t)$ is the i-th IMF, M the total number of IMFs, and $r_N(t)$ the final residual.

Since, during the sifting process, high-frequency components are firs extracted, the high-order IMFs represent fast variations, and low-order IMFs characterize slow oscillations.

In comparison to EMD, EEMD also performs the sifting process but with the elaboration that the following additionally steps are performed: (1) white noise (with a given amplitude) is added to the input signal, (2) the sifting process is performed to the new signal (raw signal + white noise), (3) steps (1) and (2) are repeated with different realizations of white noise, and (4) the ensemble mean of the corresponding IMFs of the decompositions is calculated [32]. This procedure improves EMD by avoiding the mode mixing problem (not optimal decomposition of the input signal, leading to IMFs that not represent the true oscillations component of the input signal) that can appear by applying EMD [32]. When using EEMD, two parameters are needed to be set: (i) the amplitude of the added white noise in relation to the standard deviation of the input signal (a_{std}), and (ii) the ensemble number (n). The ensemble number refers to the number of repeated sifting processes.

For the present study, an ensemble number of $n = 100$ was used by applying EEMD to the three input signal (D/Pd, T and P). The parameters a_{std} were empirically chosen for every signal so that the daily oscillation could be extracted optimally. The following values are used: a_{std}(D/Pd) = 0.5, $a_{\mathrm{std}}(T) = 2$, and $a_{\mathrm{std}}(P) = 1$.

After decomposing of each signal (D/Pd, T and P) into IMFs, we tested whether each IMF is a really a physically meaningful oscillation or only noise. The method proposed by Wu and Huang [36,37] was used. It calculated for each IMF whether it contains statistically significant information or not. For this statistical test, the rescaled energy of each IMF is calculated and compared with the theoretical white noise level.

2.5. Power spectral analysis

Power spectral analysis was applied to the signals by performing a n-point discrete Fourier transform (DFT) using the fast Fourier transform (FFT) method. For having a good frequency resolution, we choose $n = 500$.

2.6. Correlation analysis

The correlation between the signals was quantified by calculating the Pearson correlation coefficient r, which measures the linear dependency between two variables, resulting in a value in the range [–1, 1], with $r = 0$ implying that there is no linear correlation and $r = -1$ or $r = 1$ that the relationship between the two variables is perfectly described by a linear equation. The statistical significance of the correlations was computed using a t-test.

2.7. Phase synchronization analysis

In order to gain insights into how well the signals are in phase, a phase synchronization analysis was performed. The phase synchronization for two signals $x(t)$ and $y(t)$ can be calculated by a three step process [38,39]. First, the analytical signals of $x(t)$ and $y(t)$ are calculated using the Hilbert transform:

$$\psi_1(t) = x(t) + i\tilde{x}_1(t) = A_1(t)\,\mathrm{e}^{i\,\varphi_1(t)} \quad \text{and} \quad \psi_2(t) = y(t) + i\,\tilde{y}_2(t) = A_2(t)\,\mathrm{e}^{i\,\varphi_2(t)},$$

where $A_1(t)$ and $A_2(t)$ are the instantaneous phases, $\varphi_1(t)$ and $\varphi_2(t)$ the instantaneous frequencies, and $\tilde{x}_1$ and $\tilde{x}_2$ the Hilbert transforms of $x(t)$ and $y(t)$, respectively. In general, the Hilbert transform of a signal $z(t)$ is given as

$$\tilde{z}(t) = \frac{1}{\pi} PV \int_{-\infty}^{\infty} z(\tau)\frac{1}{t-\tau}\mathrm{d}\tau,$$

where PV refers to the Cauchy principal value.

In the next step, the instantaneous phase difference $\Delta\varphi(t)$ of the two signals $x(t)$ and $y(t)$ is calculate according to $\Delta\varphi(t) = \varphi_2(t) - \varphi_1(t)$.

Finally, the synchronization index $\gamma(t)$ is calculated by $\gamma(t) = \left|\mathrm{e}^{i\,\Delta\varphi(t)}\right|$. All values of $\gamma(t)$ are in the range [0, 1] where $\gamma = 1$ refers to a perfect synchronization and $\gamma = 0$ to no synchronization between the signals.

3. Results

3.1. Waveforms

Figure 1 shows the raw signals, the selected time span and the filtered version of the signals. The waveform analysis revealed that the waveforms of the daily oscillations where different in the three signals (see Fig. 2). The amplitudes of the T and P signals had a negative maximum where the waveform of D/Pd had a positive amplitude maximum. The average values for the amplitudes A of the oscillations where $A(\text{D/Pd}) \approx 2\%$, $A(T) \approx 2\,\text{K}$ and $A(P) \approx 0.06\,\text{atm}$.

3.2. EEMD and IMFs

The results of the signal decompositions are depicted in Fig. 3. It was found that for all the three signals, the second IMF was statistical significantly above the theoretical white noise level ($p = 0.05$) (see Fig. 3(d–f)). Therefore, for the further analysis the second IMF (see Fig. 3(g–i)) was used from each of the three signals.

3.3. Power spectra

The calculation of the power spectra revealed that the statistical significant oscillation (the second IMF) of the signals is a daily oscillation with a frequency of 1 d^{-1} (see Fig. 4(a–c). In order to see the effect of the filtering, the spectra where also calculated using the raw data for comparison (see Fig. 5). The additional peaks in the spectra are clear;

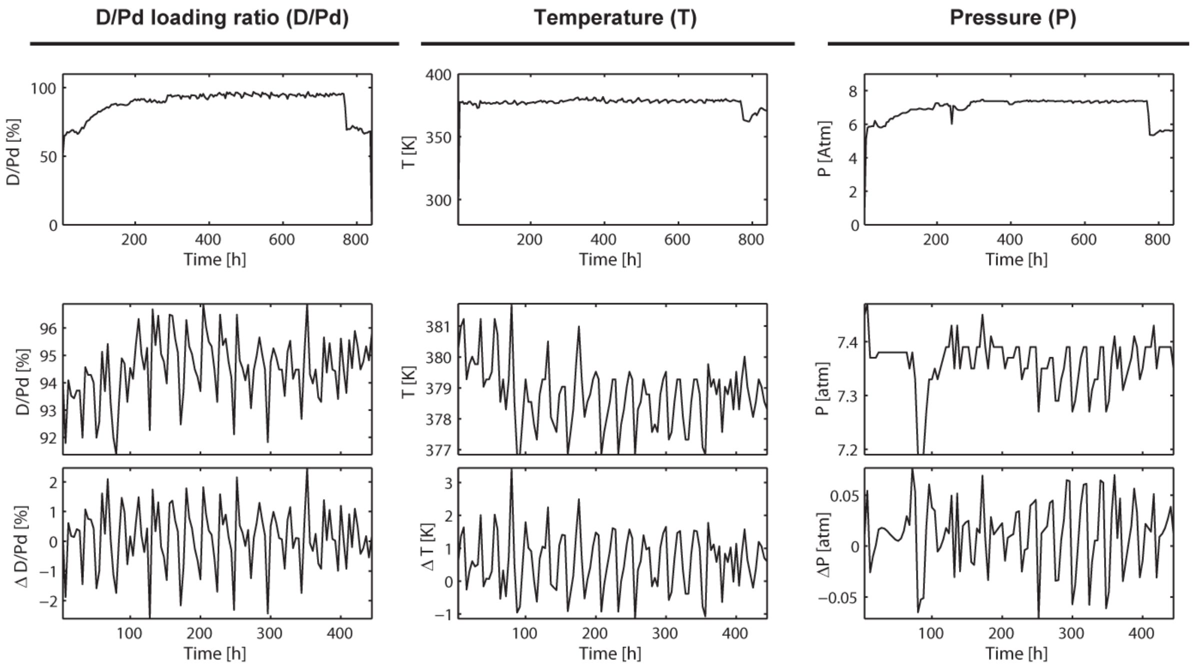

Figure 1. Raw signals (a–c), selected intervals (d–f) and results of the FIR-filtering (g–i).

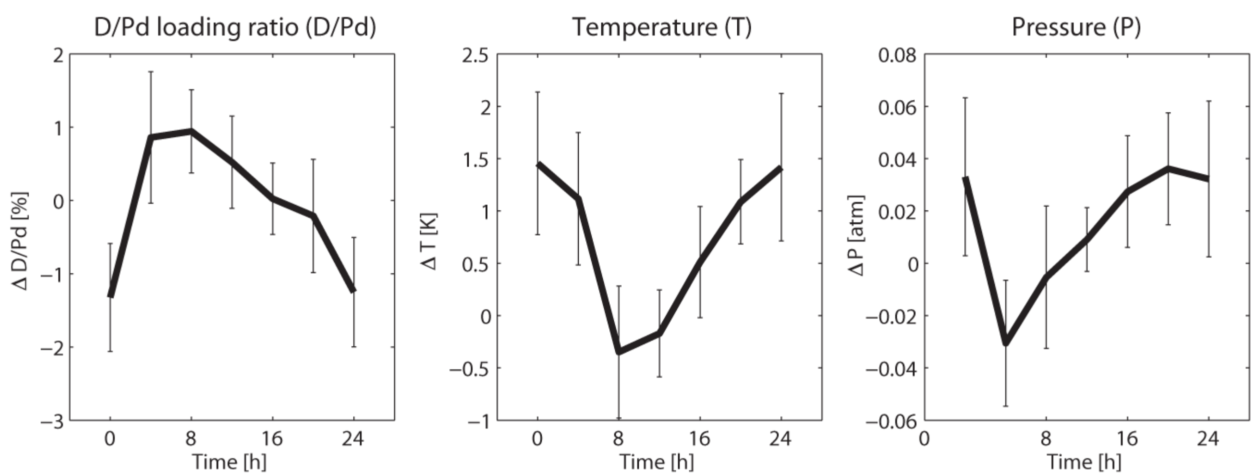

Figure 2. Block averages of the consecutive time intervals with a duration of 24 h from the three measured signals. *Bold line*: mean, error bars: ± standard deviation.

they appear at the frequencies of approx. 2 and 3 d^{-1} as well as in the low-frequency (LF) band ($< 0.5\ d^{-1}$). Only the daily oscillations where significant (as the statistical test of the IMFs indicated). Hence, one can conclude that (i) the oscillations of 2 and 3 d^{-1} are harmonics in the power spectra that are caused by the non-sinusoidal waveforms and are not own oscillations present in the signals, (ii) the LF components are non-linear trends in the signal that also do not represent a physically meaningful oscillation component of the signal.

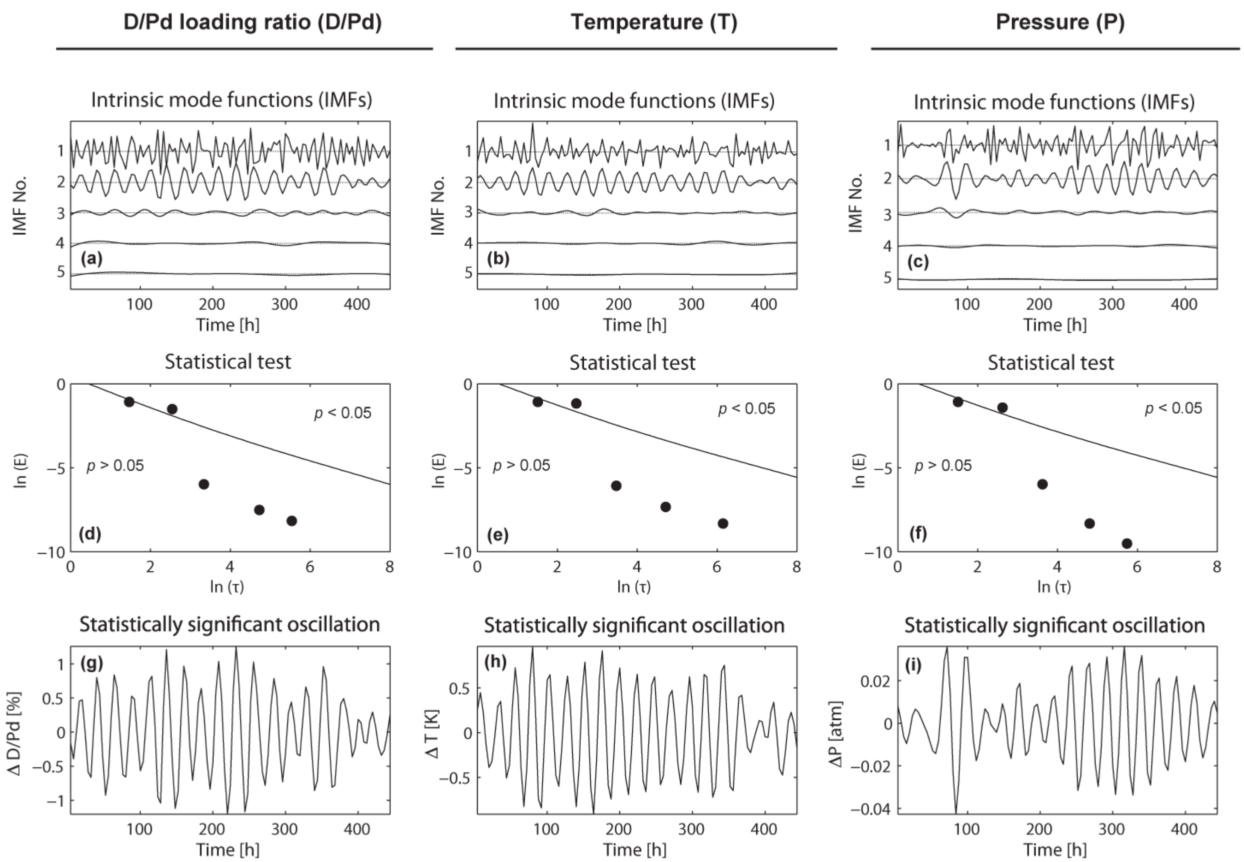

Figure 3. Results of the EEMD signal processing. IMFs (a–c), results of the statistical test (d–f) and statistically significant oscillations (g–i). The lines in the subplots (d–f) are the theoretical white noise levels with correspond to the 5% significance level ($p = 0.05$).

3.4. Correlations

As the correlation analysis showed, D/Pd and T as well as D/Pd and P were significantly negatively correlated ($r = -0.7693$, $p < 0.001$ and $r = -0.4324$, $p < 0.001$) while the correlation between T and P was significantly positive ($r = 0.307$, $p < 0.001$) (see Fig. 4(d–f)).

3.5. Phase synchronization

The analysis of the phase synchronization between the signals showed that all signals are synchronized during the whole time where the strongest synchronization was detectable between D/Pd and T (see Fig. 4(g–i)).

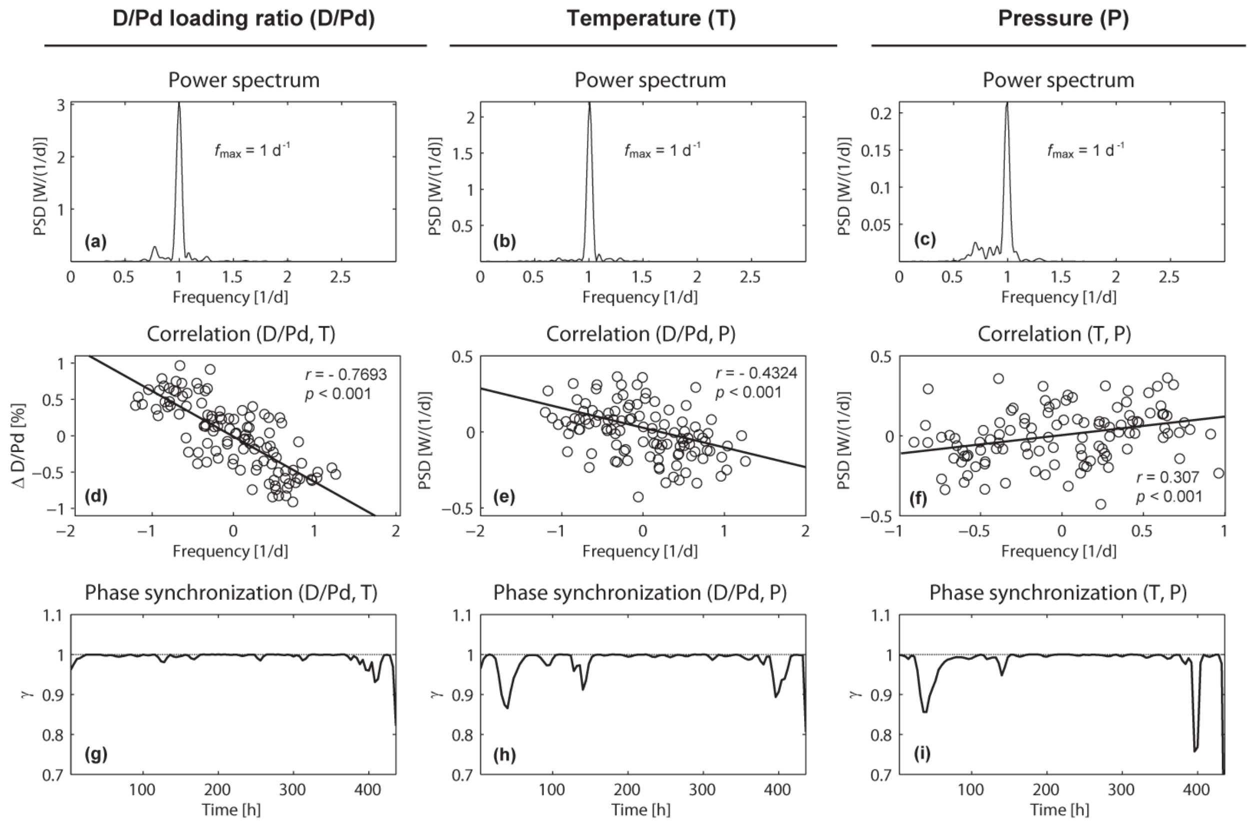

Figure 4. Power spectra (a–c), correlations (d–f) and time variations of the phase synchronizations (g–i).

4. Discussion, Conclusions and Outlook

The different methods of signal analysis performed in the present study revealed that (i) in all three signals (D/Pd, T and P) a clear daily oscillation was present (confirmed with statistical testing of the IMFs, power spectral analysis and

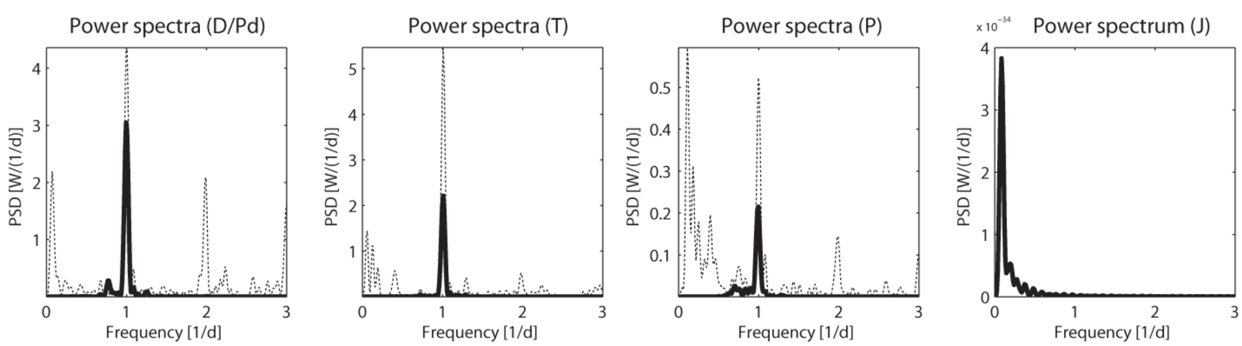

Figure 5. Power spectra calculated with the raw and filtered signals.

waveform analysis) while the current density J did not showed such an oscillation, (ii) the daily oscillation in T and P had similar waveforms and where anti-correlated to the oscillation in D/Pd, (iii) D/Pd and T had the highest correlation (r = 0.7693), (iv) all three signals exhibited phase synchronization over the whole signal length, with the strongest phase synchronization between D/Pd and T.

Concerning the possible cause of the daily oscillation one can conclude from the obtained results that it is not probably that a daily variation in the current density J caused the daily oscillations in the three other signals. That is, the power supply was stable independent over time. Also, there might be a causal relationship between D/Pd and T (since they are the best correlated). The direction of causality could not be analyzed since of the poor sampling frequency. Having an higher sampling frequency would allow performance of a causality analysis, such as the Granger causality test [40] for example.

In general, the factor causing the daily oscillation could be an internal or external one.

An internal factor could be that the electrochemical LENR dynamics exhibit characteristics of a nonlinear physiochemical oscillator, driven by the thermodynamic non-equilibrium and the composition of the reactants. Such self-oscillations where found to occur in different chemical and physiochemical reactions [41–45], where the Belousov–Zhabotinsky reaction [46] is the most famous one.

The observed daily variation could also be caused by an external factor. The most obvious factors could be a meteorological variable such as atmospheric temperature, atmospheric pressure or relative humidity. Daily oscillations are present in the fluctuations of atmospheric temperature [47], atmospheric pressure [48] and relative humidity [49]. Also the concentration changes of NO_2, O_2, O_4 [50], CO_2 [51,52] and radon [53,54] exhibit a daily oscillation.

Other external factors could be of geophysical (e.g. changes of the geomagnetic field strength and orientation) or of cosmophysical origin (e.g. changes in cosmic ray intensity and solar wind strength). Periodic geo- and cosmophysical influences were reported for different physiochemical processes. For example, Piccardi et al. [55] observed daily, annual and long-term variations in chemical reaction rates. Similar effects where found in crystallisation processes [56]. They were explained as originating mainly from low-frequency oscillations of the earth magnetic field.

Unexpected daily oscillations were also found in a world-wide network of physical random number generators [57], in the frequency drift of two quartz resonators [58] and even in the value of the gravitational constant measured using a torsion balance [59].

Interestingly, unexpected oscillations with different periods where also registered in nuclear decay process. Oscillations with daily [60–63], monthly [60,61,63] and yearly [61,63–72] periods where found. In addition, even an oscillation with a period in the range of 11–12 years could be identified [70,73] (maybe corresponding to the 11-year solar cycle).

In order to evaluate whether one of the mentioned internal and external factors caused the observed daily oscillation in this LENR experiment, further analysis has to be done. One good start would be to replicate the original LENR experiment of Mizuno et al. [5] and to optimize the experimental setup and measurement with respect to:

(1) Increasing the duration of the experiment and the measurements (suggestion: $>$ 1 month).
(2) Increasing the sampling frequency (suggestion: 1 Hz).
(3) Improving the experimental setup so that there could not be any effect from temperature, pressure and humidity on the LENR process in the flask.
(4) Continuous measuring temperature, pressure and humidity inside and outside the flask, as well as in the room where the experiment takes place.
(5) Continuous measuring of the magnetic field strength and the strength of electromagnetic radiation in different frequency bands.
(6) Performing the experiment at different global locations in order to evaluate whether the daily oscillation is dependent on the geographical location.

(7) Simultaneously performing the experiment on different locations and analyzing the time correlation of the measured parameters.
(8) Applying different kinds of shielding (e.g. lead, aluminium, mu-metal) to the experimental setup.
(9) Intentional variation of the potential influencing parameters (temperature, pressure, humidity, magnetic field strength, etc.) and analyzing their impact on the occurrence and characteristic of the daily oscillation.
(10) Performing a causality analysis between all measured parameters to determine their relationships.
(11) Measuring the D/Pd ratio with two different methods (gas and resistance method) and evaluating whether the daily oscillation is present in both parameters or not.

In conclusion, the present study investigated the observed phenomenon of a daily oscillation in an LENR experiment. No clear answer could be given regarding the origin of the daily oscillation. However, a promising signal processing framework was demonstrated. It could be employed in further analysis using data from proposed experiments, which extend the original experiment regarding the duration of the experiment and the recording of internal and external parameters. Thus, further analyses might indicate the origin of the daily oscillations in nuclear reaction rates.

References

[1] G.H. Miley, Characteristics of reaction product patterns in thin metallic films experiments, in *Asti Workshop on Anomalies in Hydrogen/Deuterium Loaded Metals*, Rocca d'Arazzo, Italy, 1997.
[2] G.H. Miley et al., Quantitative observations of transmutation products occuring in thin-film coatedmicrospheres during electrolysis, in *6th Int. Conf. on Cold Fusion*. 1996. Tokyo, Japan.
[3] G.H. Miley and J.A. Patterson, Nuclear transmutations in thin-film nickel coatings undergoing electrolysis, *J. New Energy* **1**(3) (1996) 5–39.
[4] T. Mizuno, Experimental confirmation of the nuclear reaction at low energy caused by electrolysis in the electrolyte. in *Symposium on Advanced Research in Energy Technol. 2000,* Hokkaido University, 2000.
[5] T. Mizuno, Transmutation reactions in condensed matter, in *Low-Energy Nuclear Reactions Sourcebook, American Chemical Society Symposium Series,* J. Marwan and S.B. Krivit (Eds.), DC, Oxford University Press, 2008, pp. 271–294.
[6] D.W. Mo et al., The evidence of nuclear transmutation phenomena in Pd-system using NAA, Vancouver, B.C., Canada: ENECO, University of Utah Research Park, 1998.
[7] T. Ohmori et al., Transmutation in a gold-light water electrolysis system, *Fusion Technol.* **33** (1998) 367–382.
[8] Y. Iwamura, M. Sakano and T. Itoh, Elemental analysis of Pd complexes: effects of D_2 gas permeation, *Japanese J. Appl. Phys.* **41** (2002) 4642–4648.
[9] J. Warner and J. Dash. Heat production during the electrolysis of D20 with titanium cathodes. in *8th Int. Conf. on Cold Fusion*, Bologna, Italy, 2000.
[10] M. Bernardini et al., Anomaleous effects induced by D_2O electrolysis at titanium. in *8th Int. Conf. on Cold Fusion,* Bologna, Italy, 2000.
[11] R.T. Bush and R.D. Eagleton, Evidence for electrolytically induced transmutation and radioactivity correlated with excess heat in electrolytic cells with light water rubidium salt electrolytes, *Trans. Fusion Technol*. **26**(4T) (1994) 344.
[12] J. Divisek, L. Fuerst and J. Belej, Energy balance of D_2O electrolysis with a palladium cathode. Part II. Experimental results, *J. Electroanal. Chem.* **278** (1989) 99.
[13] D. Cirillo and V. Iorio, Transmutation of metal at low energy in a cinfined plasmain water, in *11th Int. Conf. on Cold Fusion,* Marseilles, France, 2004.
[14] R. Notoya, Low temperature nuclear change of alkali metallic ions caused by electrolysis, *J. New Energy* **1**(1) (1996) 39.
[15] V.A. Romodanov, Tritium generation during the interaction of plasma glow discharge with metals and a magnetic field, in *10th Int. Conf. on Cold Fusion,* Cambridge, USA, 2003.
[16] V. Violante et al., X-ray emission during electrolysis of light water on palladium and nickel thin films, in *9th Int. Conf. on Cold Fusion,* Beijing, China, 2002.

[17] V. Violante et al., Analysis of Ni-hybride thin film after surface plasmons generation by laser technique, in *10th Int. Conf. on Cold Fusion,* Cambridge, USA, 2003.
[18] Y. Iwamura, T. Itoh and M. Sakano, Nuclear products and their time dependence induced by continous diffusion of deuterium through multi-layer palladium containing low work function material, in *8th Int. Conf. on Cold Fusion*, Bologny, Italy, 2000.
[19] J. Dash and S. Miquet, Microanalysis of Pd cathodes after electrolysis in aqueous acids, *J. New Energy* **1**(1) (1996) 23.
[20] S. Miguet and J. Dash, Microanalysis of palladium after electrolysis in heavy water, *J. New Energy* **1**(1) (1996) 23.
[21] F. Celani et al., Thermal and isotopic anomalies when Pd cathodes are electrolyzed in electrolytes, in *10th Int. Conf. on Cold Fusion*, Cambridge, USA, 2003.
[22] Y. Iwamura et al., Detection of anomaleous elements, X-ray and excess heat induced by continous diffusion of deuterium through multi-layer cathose (Pd/CaO/Pd), in *7th Int. Conf. on Cold Fusion,* Vancouver, Canada, 1998.
[23] T. Ohmori et al., Transmutation in the electrolysis of light water - excess energy and iron production in a gold electrode, *Fusion Technol.* **31** (1997) 210.
[24] T. Ohmori and M. Enyo, Iron formation in gold and palladium cathodes, *J. New Energy* **1**(1) (1996) 39.
[25] T. Mizuno, T. Ohmori and M. Enyo, Anomalous isotopic distribution in palladium cathode after electrolysis, *J. New Energy* **1**(2) (1996) 37.
[26] T. Mizuno, T. Ohmori and M. Enyo, Isotopic changes of the reaction products induced by cathodic electrolysis in Pd, *J. New Energy* **1**(3) (1996) 31–45.
[27] D.J. Nagel, T. Mizuno and D. Letts, Diurnal variations in LENR experiments, in *15th Int. Conf. of Low Energy Nuclear Reactions,* Roma, Italy, 2010.
[28] N.E. Huang et al., The empirical mode decomposition and the Hilbert spectrum for nonlinear and non-stationary time series analysis, *Pro. Roy. Soc. London Ser. a-Math. Physical and Eng. Sci.* **454** (1971) 903–995.
[29] I. Magrin-Chagnolleau and R.G. Baraniuk, Empirical mode decomposition based time-frequency attributes, in *69th SEG Meeting,* Houston, TX, USA, 1999.
[30] P. Flandrin, G. Rilling and P. Goncalves, Empirical mode decomposition as a filter bank, *IEEE Signal Process. Lett.* **11**(2) (2004) 112–114.
[31] S. Assous, A. Humeau and J.P. L'Huillier, Empirical Mode Decomposition applied to laser doppler flowmetry signals: Diagnosis approach, *27th Annual Int. Conf. of the IEEE Engineering in Medicine and Biology Society*, Vols. 1–7, 2005, pp. 1232–235.
[32] Z.H. Wu and N.E. Huang, Ensemble empirical mode decomposition: a noise assisted data analysis method, *Adv. Adaptive Data Analysis* **1**(1) (2009) 1–41.
[33] N.E. Huang, An adaptive data analysis method for nonlinear and nonstationary time series: The empirical mode decomposition and Hilbert Spectral Analysis, *Wavelet Analysis and Applications*, 2007, pp. 363–376.
[34] N.E. Huang, Review of empirical mode decomposition, *Wavelet Applications VIII* **4391** (2001) 71–80.
[35] N.E.Huang, A new method for nonlinear and nonstationary time series analysis: Empirical mode decomposition and Hilbert spectral analysis, *Wavelet Applications VII* **4056** (2000) 197–209.
[36] Z.H. Wu and N.E. Huang, A study of the characteristics of white noise using the empirical mode decomposition method, *Pro. Roy. Soc. London Series, a-Math. Physical and Eng. Sci.* **460** (2006) 1597–1611.
[37] P.X. Gao, H.F. Liang and W.W. Zhu, Periodicity of flare index revisited using the Hilbert-Huang transform method, *New Astronomy* **16**(3) (2011) 147–151.
[38] M.G. Rosenblum, A.S. Pikovsky and J. Kurths, Phase synchronization of chaotic oscillators, *Phy. Rev. Lett.* **76**(11) (1996) 1804–1807.
[39] M. Winterhalder et al., Sensitivity and specificity of coherence and phase synchronization analysis, *Phys. Lett.* A **356**(1) (2006) 26–34.
[40] C.W.J. Granger, Investigating causal relations by econometric models and cross-spectral methods, *Econometrica* **37**(3) (1969) 414–438.
[41] F. Rossi and M.L.T. Liveri, Chemical self-organization in self-assembling biomimetic systems, *Ecological Modelling* **220**(16) (2009) 1857–1864.
[42] S. Kiatiseviand and S. Maisch, Study of the oscillation and luminol chemiluminescence in the H_2O_2–KSCN–$CuSO_4$–NaOH system, *Chemical Phys. Lett.* **499**(1–3) (2010) 173–177.
[43] V.I. Nekorkin et al., Polymorphic and regular localized activity structures in a two-dimensional two-component reaction–

diffusion lattice with complex threshold excitation, *Physica D-Nonlinear Phenomena* **239**(12) (2010) 972–987.
[44] J. Horvath, I. Szalai and P. De Kepper, Pattern formation in the thiourea–iodate–sulfite system: Spatial bistability, waves, and stationary patterns, *Physica D-Nonlinear Phenomena* **239**(11) (2010) 776–784.
[45] R. Yoshida et al., Self-oscillating gel as novel biomimetic materials, *J. Controlled Release* **140**(3) (2009) 186–193.
[46] A.M. Zhabotinsky, Periodic oxidizing reactions in liquid phase, *Doklady Akademii Nauk Sssr*. **157**(2) (1964) 392–395.
[47] K.Y. Vinnikov, A. Robock and A. Basist, Diurnal and seasonal cycles of trends of surface air temperature, *J. Geophysical Research-Atmospheres* **107**(D22) (2002).
[48] V.V. Ivanov, Seasonal and diurnal variations in atmospheric pressure, *Izvestiya Atmospheric and Oceanic Phys.* **43**(3) (2007) 323–337.
[49] A. Dai et al., Diurnal variation in water vapor over North America and its implications for sampling errors in radiosonde humidity, *J. Geophysical Research-Atmospheres*. **107**(D10) (2002) ACL 11.1–11.14.
[50] G.S. Meena and D.B. Jadhav, Study of diurnal and seasonal variation of atmospheric NO_2, O_3, H_2O and O_4 at Pune, India, *Atmosfera* **20**(3) (2007) 271–287.
[51] S.B. Idso, C.D. Idso and R.C. Balling, Seasonal and diurnal variations of near-surface atmospheric CO_2 concentration within a residential sector of the urban CO_2 dome of Phoenix, AZ, USA, *Atmospheric Environment* **36**(10) (2002) 1655–1660.
[52] Y.S. Wang et al., Trend, seasonal and diurnal variations of atmospheric CO2 in Beijing, *Chinese Sci. Bulletin* **47**(24) (2002) 2050–2055.
[53] J.P. Rydock, A. Naess-Rolstad and J.T. Brunsell, Diurnal variations in radon concentrations in a school and office: implications for determining radon exposure in day-use buildings, *Atmospheric Environment* **35**(16) (2001) 2921–2926.
[54] V.R.K. Murty et al., Indoor and outdoor radon levels and its diurnal variations in Botswana, *Nucl. Inst.Methods Phys. Res.* A **619**(1–3) (2010) 446–448.
[55] G. Piccardi, *The Chemical Basis of Medical Climatology,* Springfield, Charles C. Thomas, 1962.
[56] E.A. Baranovsky, V.P. Tarashchuk and B.M. Vladimirsky, Effect of solar activity and geophysical disturbance on physical-chemical processes in liquid medium: Preliminary analysis of storm-glass activity, *Izvestiya Atmospheric and Oceanic Phys.* . **46**(8) (2010) 925–934.
[57] S.E. Shnoll and V.A. Panchelyuga, Cosmo-physical effects in the time series of the GCP network, arXiv:physics/0605064v1 [physics.gen-ph], 2006.
[58] N.V. Klochek, L.E. Palamarchuk and M.B. Nikonova, Preliminary results of investigation of the influence of cosmophysical radiation of non-electromagnetic nature on physical and biological systems, *Biofisika* **40**(4) (1995) 889–896.
[59] M.L. Gershteyn et al., Experimental evidence that the gravitational constant varies with orientation, *Gravitation and Cosmology* **8**(3) (2002) 243–246.
[60] Y.A. Baurov et al., Experimental investigations of changes in the rate of beta decay of radioactive elements, *Phys. Atomic Nuclei*. **70**(11) (2007) 1825–1835.
[61] S.E. Shnoll, K.I. Zenchenko and N.V. Udaltsova, Cosmo-physical effects in structure of the daily and yearly periods of change in the shape of the histograms constructed by results of measurements of alpha-activity Pu-239, arXiv:physics/0504092v1 [physics.space-ph], 2005.
[62] Y.V. Deshcherevskaya et al., Spectral analysis of macroscopic fluctuations in experimental time series, *Biofizika* **40**(5) (1995) 1113–1116.
[63] A.G. Parkhomov, Researches of alpha and beta radioactivity at long-term observations, arXiv:1004.1761v1 [physics.gen-ph] 2010.
[64] D.E. Alburger and G. Harbottle, Half-Lives of Ti^{44} and Bi^{207}, *Phy. Rev*. C **41**(5) (1990) 2320–2324.
[65] K.J. Ellis, The effective half-life of a broad beam (pube)-Pu-238 total-body neutron irradiator, *Phys. Medicine and Biology* **35**(8) (1990) 1079–1088.
[66] H. Siegert, H. Schrader and U. Schotzig, Half-life measurements of europium radionuclides and the long-term stability of detectors, *Appl. Radiation and Isotopes* **49**(9–11) (1998) 1397–1401.
[67] E.D. Falkenberg, Radioactive decay caused by neutrinos? *Apeiron* **8**(2) (2001) 32–45.
[68] D.E. Alburger, G. Harbottle and E.F. Norton, Half-life of ^{32}Si, *Earth and Planetary Sci. Lett.* **78**(2–3) (1986) 168–176.
[69] P.A. Sturrock et al., Power Spectrum Analysis of Physikalisch-Technische Bundesanstalt Decay-Rate Data: Evidence for Solar Rotational Modulation, *Solar Phys.* **267**(2) (2010) 251–265.

[70] D. Javorsek et al., Power spectrum analyses of nuclear decay rates, *Astroparticle Phys.* **34**(3) (2010) 173–178.
[71] J.H. Jenkins et al., Evidence of correlations between nuclear decay rates and Earth-Sun distance, *Astroparticle Phys.* **32**(1) (2009) 42–46.
[72] J.H. Jenkins, D.W. Mundy and E. Fischbach, Analysis of environmental influences in nuclear half-life measurements exhibiting time-dependent decay rates, *Nucl. Instr. Methods Phys.* A **620**(2–3) (2010) 332–342.
[73] P.A. Sturrock et al., Power spectrum analysis of BNL decay rate, *Astroparticle Phys.* **34**(2) (2010) 121–127.